A Scale-Dependent Quality Index of Areal Rainfall Prediction

Eddy Yates, Jean-Dominique Creutin, Sandrine Anquetin, Jacques Rivoirard

A Scale-Dependent Quality Index of Areal Rainfall Prediction

EDDY YATES, JEAN-DOMINIQUE CREUTIN, AND SANDRINE ANQUETIN

Laboratoire d'étude des Transferts en Hydrologie et Environnement, Grenoble, France

JACQUES RIVOIRARD

Centre de Géostatistique, Ecole des Mines de Paris, Fontainebleau, France

ABSTRACT

Many performance indexes have been proposed to assess the quality of predicted rainfall fields. Each new index is generally tested on schematic cases or on case studies. A quality index of predicted rainfall fields is proposed based on the evolution versus scale of the correlation between observed and predicted areal rainfalls, for different scales of integrating surfaces. The authors examine this quality index with both an analytical and a numerical approach. The geostatistical structure of the rainfall field is assumed known. The index generally shows a fast increase around a scale, which is called "critical scale."

The effect on this index of a bad localization of the predicted field is to change the critical scale, and there is a simple link between the shift and this critical scale. This link depends on the short-range structure of the rainfall field for small shifts.

The effect of having a reference known only by point measures and interpolation is a decrease of the index. An even repartition of the rain gauges improves the index. The critical scale for a perfectly localized simulation corresponds to a surface containing one rain gauge. If the simulation is badly localized, the index cannot see the bad localization if the shift is smaller than the distance between two rain gauges.

1. Introduction

This paper deals with the multiscale validation of predicted regionalized variables, for example, the rainfall fields simulated by meteorological models. The validation of simulated fields requires a reference, such as the readings from a rain gauge network, and the definition of a performance index, measuring the distance between the simulated and the reference fields. Many methods for assessing the performance of models have been proposed. Each index measures a part of the difference between the simulated and the reference fields. For example, the bias measures the tendency to over- or underestimate. The correlation measures the ability to reproduce the structure. The probability of detection (Ducrocq et al. 2002) evaluates the ability of the model to predict how often a threshold is reached. The false-alarm ratio (Mason 1989) detects if the model reaches a threshold too often. Some more refined amplitude-based performance indexes take into account both the mean and the variability of the fields, such as the universal image quality index (Wang and Bovik 2002). Others are particularly adapted to the specific properties of the rainfall fields and are based on the distance between observed and simulated patterns of rainy zones, such as the Hausdorff distance (Huttenlocher et al. 1999). Venugopal and Foufoula-Georgiou (2005) propose the forecast quality index, which combines amplitude-based and distance-based measures. The present paper focuses on the structure of the field, and therefore the correlation is used to compare the reference and the simulation.

As shown by Zepeda-Arce et al. (2000), a multiscale comparison is sometimes needed, as simulations may be considered poor when compared to a reference at the scale of the grid mesh or the point measurements, but may be considered satisfactory when the comparison is made on the basis of averages over larger areas. Such a distinction between scales is of importance, for example, for hydrologic purposes, in relation to the aggregating role of the watersheds on the rainfall field. In

Corresponding author address: Eddy Yates, Laboratoire d'étude des Transferts en Hydrologie et Environnement, BP 53, 38 041 Grenoble CEDEX 09, France.
E-mail: eddy-yates@yahoo.fr

a previous paper, Yates et al. (2006) used a quality index based on the evolution versus scale of the correlation coefficient to evaluate two simulations of intense precipitation events.

The indexes proposed in the literature are often tested on simple schematic cases or on case studies. In the present paper, an analytical approach (completed with a numerical solving of the results) is proposed to evaluate the impact of a geographical shift on the simulated rain pattern and the impact of the quality of the rain gauge network on this quality index. We present the formulation of the index in section 2. The aim of section 3 is to point out the signature of a bad geographical localization of the simulated field. This is a usual problem observed with rain fields predicted by meteorological models. Section 4 deals with the effects of using a reference field kriged from point measurements when rain gauge readings are used as reference. Tustison et al. (2001) show that the representativeness errors (i.e., the error in representing data at a scale other than their own inherent scale) produced by using point measurements to validate areal rainfalls, need to be known at each scale. In this section we show first the signature of the density of the rain gauge network on the quality index. We finally illustrate the possibility of detecting bad localizations with a kriged reference.

2. The quality index

We consider rain fields as realizations of a random function that verify the intrinsic hypothesis (see appendix A). We define two rain fields, a reference field z and a simulated field ζ, on a domain $\mathcal{D}$. The surface area of $\mathcal{D}$ is D, and its limits are $0 \leq x \leq \sqrt{D}$ and $0 \leq y \leq \sqrt{D}$. The domain $\mathcal{D}$ can be paved with square-shaped surfaces S_k ($k \in \{1, \ldots, N_s\}$), identical to a generic S. The domain is entirely covered by these surfaces; therefore, the surface area of each surface is $s = D/N_s$. The areal rainfall over each of these surfaces, that is, the mean of the rain field over these surfaces, is $z(S_k)$ for the reference and $\zeta(S_k)$ for the simulation. As k varies in $\{1, \ldots, N_s\}$, it generates two families of areal rainfalls, z_s and ζ_s. The correlation between these two families can be computed. It is a function of the scale s, within the domain $\mathcal{D}$,

$$R^2_{z,\zeta}(s|\mathcal{D}) = \left[\frac{\mathrm{Cov}(z_s, \zeta_s|\mathcal{D})}{\sigma(z_s|\mathcal{D})\sigma(\zeta_s|\mathcal{D})} \right]^2. \tag{1}$$

Here Cov stands for the covariance and σ^2 for the variance. This function $R^2_{z,\zeta}(s|\mathcal{D})$ defines a scale-dependent quality index of areal rainfall prediction.

3. Signature of a bad localization

a. Expression of the index as a function of the variogram of the rain field

In this section, we deal with the case of a mere geographical shift between the simulated field and the reference field. The "simulated field" is the rain field obtained by shifting the reference field. If the shift is denoted $\mathbf{d}$, the simulated field is derived from the reference field by $\zeta(\mathbf{x}) = z(\mathbf{x} - \mathbf{d})$, with $z(\mathbf{x})$ and $\zeta(\mathbf{x})$ the rain fields at the position $\mathbf{x}$. Therefore, z and ζ share some statistical properties, namely, both verify the intrinsic hypothesis and they have the same variogram $\gamma_z(\mathbf{h}) = \gamma_\zeta(\mathbf{h}) = \frac{1}{2}E\{[z(\mathbf{x} + \mathbf{h}) - z(\mathbf{x})]^2\}$. The variogram allows computing the variances of the z_s's within $\mathcal{D}$, thanks to the basic formula (Matheron 1965, p. 135; Chiles and Delfiner 1999, p. 131)

$$\sigma^2(z_s|\mathcal{D}) = \overline{\gamma_z(\mathcal{D}, \mathcal{D})} - \overline{\gamma_z(S, S)}, \tag{2}$$

with, for instance,

$$\overline{\gamma_z(\mathcal{D}, \mathcal{D})} = \frac{1}{D^2} \iint_{(\mathbf{x},\mathbf{y}) \in \mathcal{D}^2} \gamma_z(\mathbf{y} - \mathbf{x}) \, d\mathbf{x} \, d\mathbf{y}.$$

The variance of the simulated areal rainfalls can be written similarly, as z and ζ have the same variogram

$$\sigma^2(\zeta_s|\mathcal{D}) = \overline{\gamma_z(\mathcal{D}, \mathcal{D})} - \overline{\gamma_z(S, S)}. \tag{3}$$

The covariance of the observed and simulated areal rainfalls can be written

$$\begin{aligned} \mathrm{Cov}(z_s, \zeta_s|\mathcal{D}) &= E[(z_s - z_D)(\zeta_s - \zeta_D)] \\ &= E[(z_s - z_D)(z_{s,-\mathbf{d}} - z_{D,-\mathbf{d}})], \end{aligned}$$

with $z_{s,-\mathbf{d}}$ the family of areal rainfall on surfaces shifted by $-\mathbf{d}$. This can be developed in terms of the variogram (Matheron 1965, p. 133). The covariance is finally

$$\mathrm{Cov}(z_s, \zeta_s|\mathcal{D}) = \overline{\gamma_z(\mathcal{D}, \mathcal{D}_{-\mathbf{d}})} - \overline{\gamma_z(S, S_{-\mathbf{d}})}. \tag{4}$$

The insertion of Eqs. (2)–(4) in Eq. (1) yields

$$R^2_{z,\zeta}(s) = \left[\frac{\overline{\gamma_z(\mathcal{D}, \mathcal{D}_{-\mathbf{d}})} - \overline{\gamma_z(S, S_{-\mathbf{d}})}}{\overline{\gamma_z(\mathcal{D}, \mathcal{D})} - \overline{\gamma_z(S, S)}} \right]^2. \tag{5}$$

b. Behavior of the index for various variograms of the rain field

We compute numerically the index for different shift values, following Eq. (5). For this purpose, we use three isotropic variogram models (Fig. 1) (Chiles and Delfiner 1999). Let r be $|\mathbf{h}|$. The spherical variogram is given
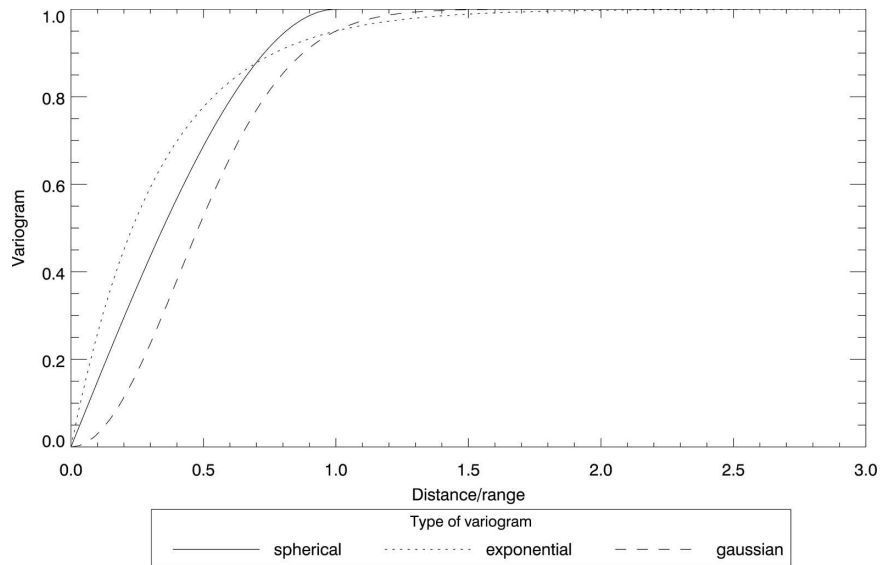
FIG. 1. Variograms.

by $\mathrm{Sph}(r) = (3r/2a) - (r^3/2a^3)$ if $r \leq a$, else $\mathrm{Sph}(r) = 1$, the exponential variogram by $\mathrm{Exp}(r) = 1 - e^{-3(r/a)}$, the Gaussian variogram by $\mathrm{Gau}(r) = 1 - e^{-3(r^2/a^2)}$ (a is the practical range of the variogram). The computation is made on an infinite domain. That means that the terms $\overline{\gamma_z(\mathcal{D}, \mathcal{D}_{-\mathbf{d}})}$ and $\overline{\gamma_z(\mathcal{D}, \mathcal{D})}$ are equal to one (the asymptotic value of the variogram).

Figure 2 displays the index curves computed following Eq. (5) for different geographical shifts. The plots use adimensional shift values (based on the range a) and scale values (based on a^2). All the curves have the same shape throughout the different shifts; there are two sills for small and large scales, separated by a zone with a fast increase of the correlation. This zone contains an inflexion point of the curve at a scale, which we call the "critical scale."

Figure 3 displays some of the results of Fig. 2, but it allows a comparison between the variogram types. For large scales, the correlation hardly depends on the variogram model. But for small scales, the correlation is better when the variogram is lower for short distances (Gaussian model, then spherical model, then exponential model; see Fig. 1). This result is intuitive: the short-range behavior of the variogram is sensitive only on small scales.

The dependence of the critical scale on the shift is shown in Fig. 4 (the critical scale is defined as the inflexion point, which is found by twice differentiating the index with respect to its abscissa, i.e., the logarithm of the scale). It must be noted that the spherical model produces two inflexion points for small shifts (up to more than a quarter of the range), which is difficult to

interpret, especially in terms of practical consequences for the validation process. Then the smaller inflexion point disappears. More important, the critical scale strongly depends on the variogram type for shifts smaller than about $0.8a$ (where a is the practical range of the variogram). Therefore, if the shift is smaller than $0.8a$, it can be determined through the index only if the type of the variogram is known.

For shifts greater than $0.8a$, the critical scale versus shift log–log curve is well approximated by a straight line (see Table 1). The slope is greater than 2, which means that the side length of the critical scale must grow faster than the shift. The slope is not very different from one variogram type to another. Therefore, the index can be used safely when the shift is greater than $0.8a$, without knowing about the type of the variogram.

4. Signature of the kriging errors

a. Expression of the index as a function of the variogram of the rain field

In this section, we call z^* the reference rain field obtained by extracting n_r point values of the observed field and by block-kriging these point values (see appendix A for explanation).

The simulated field remains the original field shifted, as in section 3. Equation (1) becomes

$$R^2_{z^*,\zeta}(s|\mathcal{D}) = \left[\frac{\mathrm{Cov}(z^*_s, \zeta_s|\mathcal{D})}{\sigma(z^*_s|\mathcal{D})\sigma(\zeta_s|\mathcal{D})} \right]^2. \qquad (6)$$
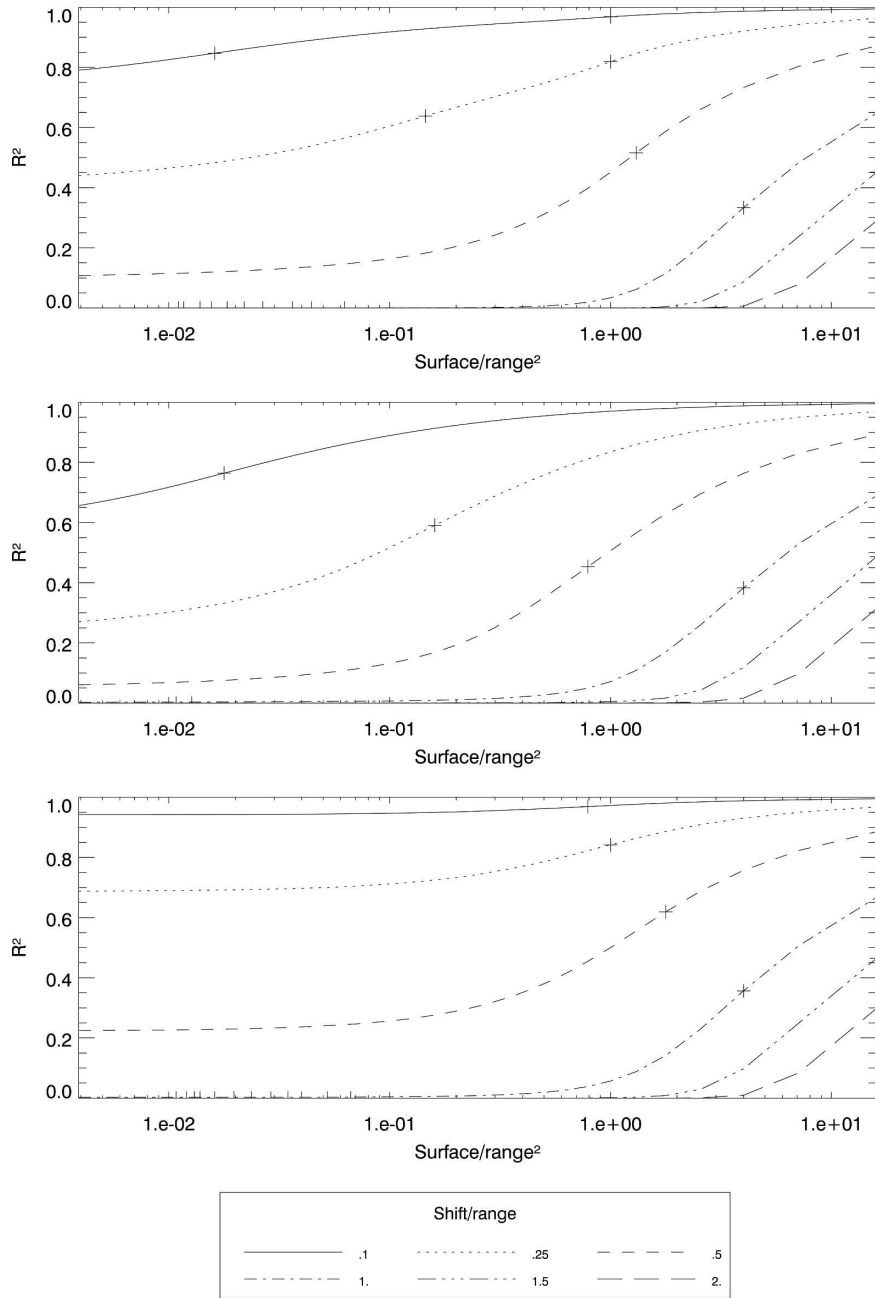
FIG. 2. Index for different shifts between the simulated field and the reference field for the three variogram types: (top) spherical, (center) exponential, and (bottom) Gaussian. The crosses indicate the critical scale.

For clarity, the developments and final formula are given in appendix C to appendix E.

b. Behavior of the index for regular rain gauge networks, with a perfect simulation (no shift)

We compute the index numerically following Eq. (E1). The results are presented in Fig. 5. We use only the spherical variogram model because of the large computation time. For the same reason, the square domain has a side length limited to eight ranges. We use four regular rain gauge networks, with different distances (d) between the gauges.

Again, we observe two sills, a sill of low correlation for small scales and a sill of high correlation for large
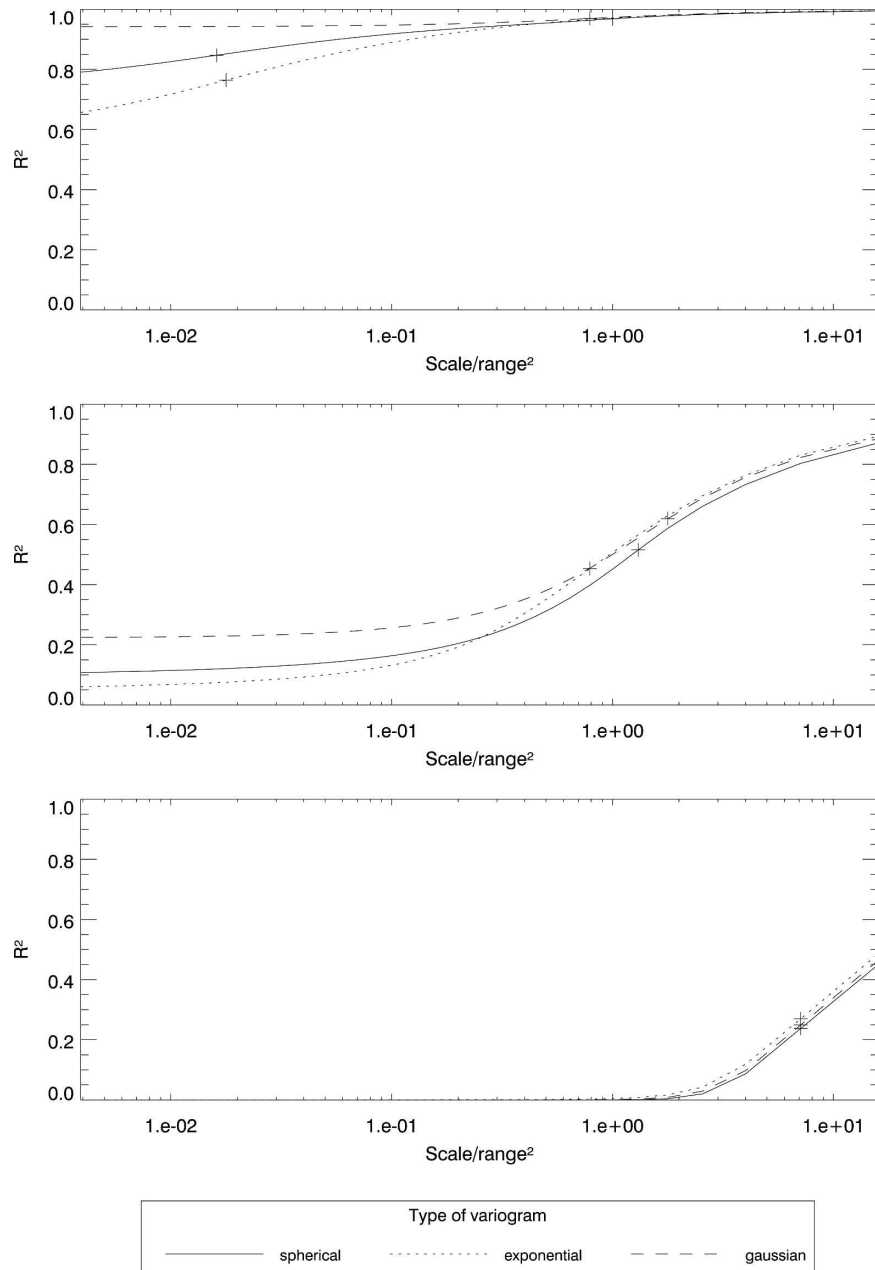
FIG. 3. Index for three different shifts between the simulated field and the reference field for the three variogram types. The ratio shift/range is 0.1 in the top diagram, 0.5 in the center diagram, and 1.5 in the bottom diagram. The crosses indicate the critical scale.

scales. Nevertheless, this is barely visible for the coarsest rain gauge networks because there is no surface large enough. These sills are separated by a fast increase of the correlation. This increase occurs at scales where the surfaces contain about one rain gauge (this is clear at least for the two best networks). This can be interpreted as follows: when the surfaces contain less than one rain gauge, the variability of the reference field is not caught by the rain gauge network, but, as the

simulation is perfect, it reproduces this variability; the correlation is therefore weak. But if the interest is on surfaces containing at least one rain gauge, the rain gauge network is able to catch the variability, and a part of the variability of the simulation is erased due to the averaging on surfaces, and therefore the correlation is better.

The curves present peaks for surfaces containing 1 [i.e., $(s/a^2) = 0.25$ for $d = (a/2)$, $(s/a^2) = 1$ for $d = a \ldots$],
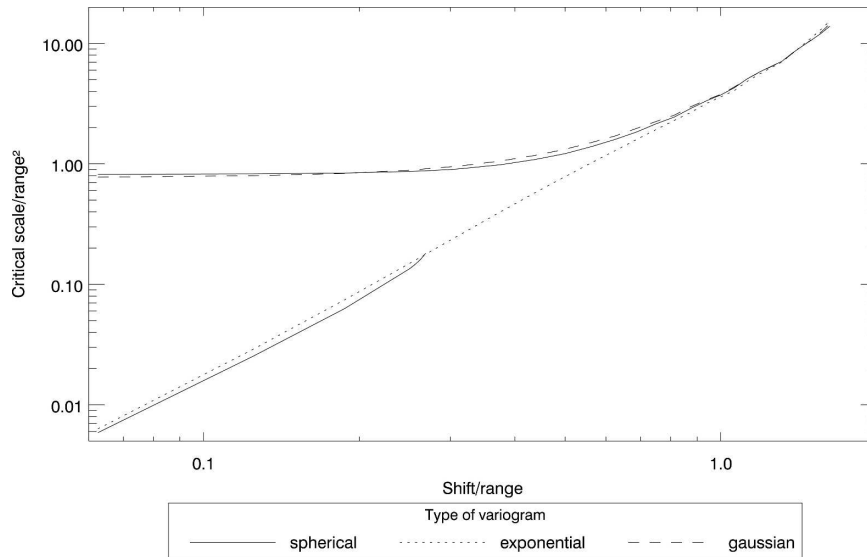
FIG. 4. Evolution of the critical scale with the shift.

4, 16 . . . rain gauges. This might be due to a special position of the integrating surfaces on the rain gauge network. This effect can be partially studied with non-regular networks.

c. Behavior of the index for nonregular rain gauge networks, with a perfect simulation (no shift)

In this section, the density of rain gauges is the same as the one with a distance between the gauges equal to the range of the variogram in section 4b, but the gauges are not localized on a regular grid. Figure 6 shows schematically the design used for the networks. The network presented in Fig. 6a is the regular one used previously. The network presented in Fig. 6f is obtained by taking random coordinates for each rain gauge. The other networks leave one-quarter (Fig. 6b), three-quarters (Fig. 6e), or one-half, with different distributions (Figs. 6c and 6d) of the domain without any rain gauge.

The index is shown in Fig. 7. An even distribution of the rain gauges improves the correlation and maintains this improvement until the largest scales; the result is better when the network is spread over the whole do-

TABLE 1. Linear regression of the 14 last points (shift/range $\geq$ 0.8) of the critical scale vs shift log–log curve.

Type of variogram	Slope	Correlation coefficient (ρ^2)
Spherical	2.48	0.994
Exponential	2.70	0.989
Gaussian	2.46	0.989

main (network a) rather than on three-quarters (network b), even better than on a half (networks c and d), and even better than on one-quarter (network e). This effect seems to be less important than multiplying the distance between the gauges by two, since the worse network (e) gives better results than the coarser network with a distance equal to two ranges in Fig. 5.

The networks c to e show a decrease of the correlation for the largest scales (this same phenomenon is not clear with the network b). For the small scales, the effect of the empty zones of the domain is partly balanced by the local higher resolution of the network. The variability is in general not reproduced, but it is better reproduced where there are rain gauges. As the scale increases, the effect of the empty zones is not balanced anymore; the local better description of the variability is erased by the aggregation.

The networks c and d, which are spread over half of the domain, have very similar results. There is a small difference for the largest scales, where the network d seems to be a little better. The network d's being a little better than c can be explained as follows: there is less overlap between the influence zone of each rain gauge in d than in c. There is, therefore, a larger zone of the domain covered by the influence of the network d.

The peaks for 1, 4 . . . rain gauges per surface remain for the networks using a grid (a to d at least). They disappear for the "random" network (f). This confirms that this is an effect of a special position of the integrating surfaces on the rain gauge network. When discussing about the index, we can therefore make as if these peaks did not exist. For this particular "random"
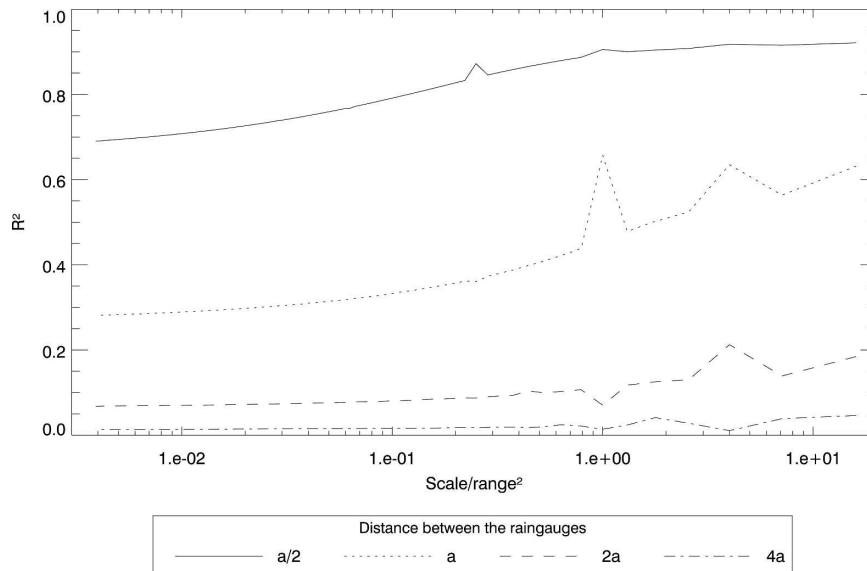
FIG. 5. Evolution of the index for four rain gauge densities.

network, the results are similar to the results with half of the domain covered by the rain gauges, at least for the smallest scales. This might be different for another random network.

d. Behavior of the index with a shifted simulation and a kriged reference

In this section, several shifts are applied to the field to obtain the simulated fields. The reference field is obtained by kriging. A regular network is used. The distance between the gauges is equal to the range of the variogram. As we discuss only the shape of the index (not the critical scale), we also use some shifts that might produce two inflexions points. The correlation is computed numerically, and the results are shown in Fig. 8.

As stated before, the peaks in Fig. 8 must not be taken into account. The comparison between Figs. 8 and 2 shows an overall reduction of the correlation when the reference is kriged (an infinite domain was used to obtain the results shown in Fig. 2, but the re-
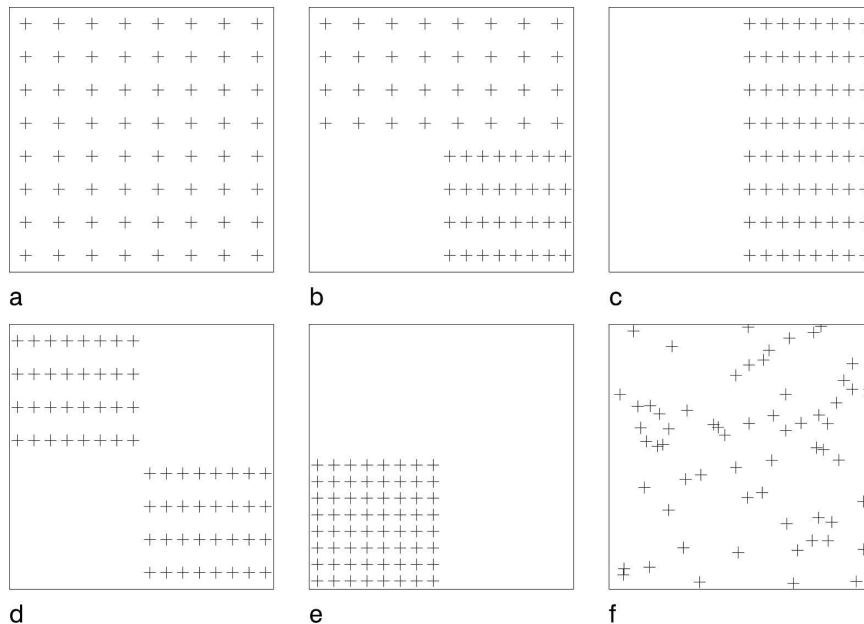

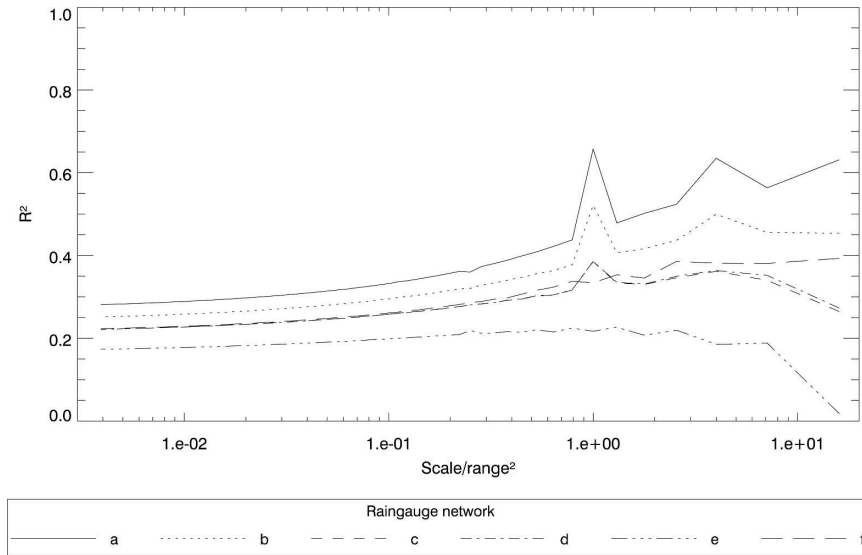FIG. 6. The six nonregular rain gauge networks.

FIG. 7. Evolution of the index for the six nonregular rain gauge networks.

sults, not shown, are very similar with a domain with a size that equals eight ranges). If the shift is smaller than the distance between the rain gauges, the critical scale corresponds to surfaces containing one gauge [i.e., $(s/a^2) = 1$, since the distance between two gauges is the range]. Therefore, the index is not sensitive to the shift of the simulations, as the critical scale is the same as if there were no shift. If the shift is larger than the distance between the rain gauges, the pattern of the curves is quite the same as in Fig. 2. This shows that the quality of the observing device (in that case, the spacing of

sampling) limits the use of this index, and therefore limits the capacity to properly validate a simulated rain field.

5. Conclusions

We propose a quality index based on the evolution versus scale of the correlation coefficient between reference and simulated areal rainfall fields integrated on surfaces of increasing size. The behavior of this scale-dependent index is analyzed with a theoretical ap-
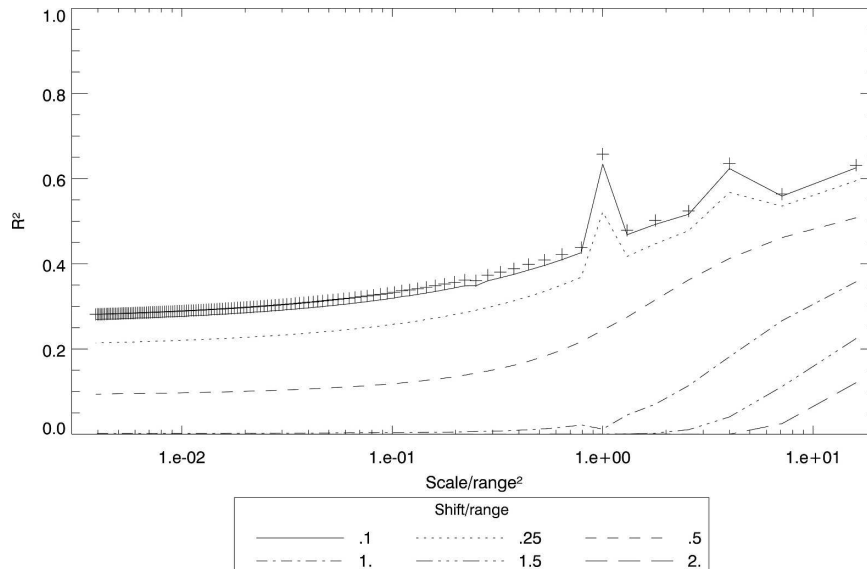

FIG. 8. Index for different shifts with a kriged reference. The crosses indicate the index without shift.

proach considering mere geographical shifts between the tested field and the reference. The reference is considered as perfect or derived from a rain gauge network by kriging. The more general shape taken by the index is a flat "S" with a fast increase of the correlation for a size of the averaging surfaces, which we call "critical scale." This critical scale depends both on the shift and on the structure of the rainfall field if the shift is smaller than $0.8a$ (where a is the practical range of the variogram). The critical scale depends only on the shift when it is larger than $0.8a$.

The use of a kriged field as a reference to evaluate a badly located simulated field is informative only if the bad localization exceeds the distance between the rain gauges. The amplitude and the level of the "S" shape vary with different configurations and densities of the rain gauge network. The representativeness errors decrease when the integrating surfaces contain at least one rain gauge. The shape of the index is less affected by the configuration of the network than by the density of the rain gauge network.

The proposed index is well suited to this type of quasi-analytical approach. It provides equations that can be solved numerically and allows testing simple errors of a simulation model. The most severe limitation concerns the types of error produced by a meteorological model. The proposed approach assumes known errors that can be mathematically formulated. Geographical shifts are obviously good candidates, being mathematically tractable and meteorologically meaningful. Other simple geometrical transformations like rotations and scaling are less realistic. More complex alterations of the rain patterns could be represented by random error fields, provided that their properties can be assessed realistically.

The present study explores a rather limited set of possibilities in terms of rain gauge network geometry, rainfall field structure, and simulation errors. Other network geometries could be tested in a straightforward manner through the same approach. The presented results could be extended to anisotropic rain fields through a mere geometric transformation of the coordinates. More sophisticated descriptions of the rain field structure, combining for instance intermittency and intrinsic variability (Barancourt et al. 1992), would be more difficult to implement, adding complexity to the various covariance descriptions. Considering these difficulties, the test of the index could be based on real fields, as it is sometimes done in the literature. Performing tests on fields generated stochastically could be another solution; moreover, it would allow a statistical study, since such field simulators can generate a huge number of fields.

APPENDIX A

Kriging

Kriging is an interpolation system that sees the rain field as a realization of a random function. If the intrinsic hypothesis (Chiles and Delfiner 1999) is verified {i.e., the temporal mean does not depend on the location and the variogram $\gamma(\mathbf{d}) = (\frac{1}{2})E\{[z(\mathbf{x} + \mathbf{d}, k) - z(\mathbf{x}, k)]^2\}$, E being the expectation and k the realization of the random function, does not depend on the location $\mathbf{x}$}, kriging allows interpolating point measurements to obtain means over surfaces. It is a linear interpolator, which means that each rain depth can be written (the realization, or time, being fixed)

$$z^*(S) = \sum_{i=1}^{n_r} \lambda_i(S)z_i,$$

with n_r the number of rain gauges, z_i the measurement of the ith rain gauge located at $\mathbf{x}_i$, and $\lambda_i(S)$ the weight associated to the ith rain gauge to compute the rain depth $z^*(S)$ over the surface S.

Kriging is an optimal, nonbiased estimator. These two attributes yield the kriging system

$$\begin{pmatrix} \gamma_{11} & \cdots & \gamma_{n_r 1} & 1 \\ & \ddots & & \\ \vdots & \gamma_{ji} & \vdots & \vdots \\ & & \ddots & \\ \gamma_{1n_r} & \cdots & \gamma_{n_r n_r} & 1 \\ 1 & \cdots & 1 & 0 \end{pmatrix} \begin{pmatrix} \lambda_1(S) \\ \vdots \\ \lambda_j(s) \\ \vdots \\ \lambda_{n_r}(S) \\ -\mu(S) \end{pmatrix} = \begin{pmatrix} \overline{\gamma(\mathbf{x}_1, S)} \\ \vdots \\ \overline{\gamma(\mathbf{x}_i, S)} \\ \vdots \\ \overline{\gamma(\mathbf{x}_{n_r}, S)} \\ 1 \end{pmatrix},$$

that is, using a matrix notation

$$\mathcal{K}\mathcal{L}(S) = \Gamma(S). \tag{A1}$$

In the matrix $\mathcal{K}$, $\gamma_{ji} = \gamma(\mathbf{x}_j - \mathbf{x}_i)$ ($\mathcal{K}$ is therefore symmetric). In the vector $\Gamma(S)$, $\overline{\gamma(\mathbf{x}_i, S)} = (1/s)\int_{\mathbf{x} \in S} \gamma(\mathbf{x} - \mathbf{x}_i)$ $d\mathbf{x}$. Here $\mu(S)$ can be shown to be $\sum_{i=1}^{n_r}\sum_{j=1}^{n_r}\lambda_i(S)\lambda_j(S)\gamma_{ji} - \sum_{i=1}^{n_r}\lambda_i(S)\overline{\gamma(\mathbf{x}_i, S)}$.

APPENDIX B

Some Useful Results

Here are some useful results used in the paper: $\{S_k, k = 1 \ldots N_s\}$ being a perfect paving of $\mathcal{D}$ yields

$$\frac{1}{N_s} \sum_{i=1}^{N_s} \overline{\gamma(i,S_k)} = \frac{1}{N_s} \sum_{i=1}^{N_s} \frac{1}{s} \int_{x \in S_k} \gamma(\mathbf{x} - \mathbf{x}_i)\, dx$$

$$= \frac{1}{D} \int_{x \in \mathcal{D}} \gamma(\mathbf{x} - \mathbf{x}_i)\, dx = \overline{\gamma(i, \mathcal{D})}.$$

(B1)

As a consequence

$$\frac{1}{N_s} \sum_{i=1}^{N_s} \Gamma(S_k) = \Gamma(\mathcal{D})$$

(B2)

and, using Eq. (A1)

$$\frac{1}{N_s} \sum_{i=1}^{N_s} \mathcal{L}(S_k) = \mathcal{K}^{-1} \frac{1}{N_s} \sum_{i=1}^{N_s} \Gamma(S_k) = \mathcal{L}(\mathcal{D}).$$ (B3)

This yields

$$\mu(\mathcal{D}) = \frac{1}{N_s} \sum_{k=1}^{N_s} \mu(S_k) \quad \lambda_i(\mathcal{D}) = \frac{1}{N_s} \sum_{k=1}^{N_s} \lambda_i(S_k),$$

and the kriging of $\mathcal{D}$ is the average of the krigings of the S_k's

$$z^*(\mathcal{D}) = \frac{1}{N_s} \sum_{k=1}^{N_s} z^*(S_k).$$

APPENDIX C

Variance of the Kriged Areal Rainfalls

By definition, the variance of the kriged areal rainfall is

$$\sigma^2(z_s^*|\mathcal{D}) = E\left\{ \frac{1}{N_s} \sum_{k=1}^{N_s} [z^*(S_k) - z^*(\mathcal{D})]^2 \right\}$$

$$= E\left\{ \frac{1}{N_s} \sum_{k=1}^{N_s} \left[\sum_{i=1}^{n_r} \lambda_i(S_k) z_i - \sum_{i=1}^{n_r} \lambda_i(\mathcal{D}) z_i \right]^2 \right\}.$$

(C1)

The expression can be developed, in terms of the variogram

$$\sigma^2(z_s^*|\mathcal{D}) = -\frac{1}{N_s} \sum_{k=1}^{N_s} \sum_{i=1}^{n_r} \sum_{j=1}^{n_r} [\lambda_i(S_k) - \lambda_i(\mathcal{D})][\lambda_j(S_k) - \lambda_j(\mathcal{D})]\gamma_{i,j}.$$

Using Eq. (B3) in appendix B yields

$$\sigma^2(z_s^*|\mathcal{D}) = \sum_{i=1}^{n_r} \sum_{j=1}^{n_r} \lambda_i(\mathcal{D})\lambda_j(\mathcal{D})\gamma_{i,j}$$

$$- \sum_{i=1}^{n_r} \sum_{j=1}^{n_r} \gamma_{i,j} \frac{1}{N_s} \sum_{k=1}^{N_s} \lambda_i(S_k)\lambda_j(S_k).$$

Equation (A1) in appendix A and appendix B yields

$$\sigma^2(z_s^*|\mathcal{D}) = \mu(\mathcal{D}) - \frac{1}{N_s} \sum_{k=1}^{N_s} \mu(S_k) + \sum_{i=1}^{n_r} \lambda_i(\mathcal{D})\overline{\gamma(i,\mathcal{D})}$$

$$- \frac{1}{N_s} \sum_{k=1}^{N_s} \sum_{i=1}^{n_r} \lambda_i(S_k)\overline{\gamma(i,S_k)}.$$

Using a matrix notation and Eq. (B3) in appendix B

$$\sigma^2(z_s^*|\mathcal{D}) = \frac{1}{N_s} \sum_{k=1}^{N_s} \mathcal{L}^{\mathrm{T}}(S_k)[\Gamma(\mathcal{D}) - \Gamma(S_k)].$$

Finally, Eq. (A1) in appendix A yields

$$\sigma^2(z_s^*|\mathcal{D}) = \frac{1}{N_s} \sum_{k=1}^{N_s} \Gamma^{\mathrm{T}}(S_k)\mathcal{K}^{-1}[\Gamma(\mathcal{D}) - \Gamma(S_k)].$$

(C2)

APPENDIX D

Covariance between the Kriged and the Shifted Areal Rainfalls

The covariance $\mathrm{Cov}(z_s^*, \zeta_s|\mathcal{D})$ can be written, since the simulation is obtained by shifting the actual rain field,

$$\mathrm{Cov}(z_s^*,\zeta_s|\mathcal{D}) = \frac{1}{N_s} \sum_{k=1}^{N_s} E\{[z^*(S_k) - z^*(\mathcal{D})][z(S_{k-\mathbf{d}})$$

$$- z(\mathcal{D}_{-\mathbf{d}})]\}.$$

The estimated rain depth is a linear combination of the measures; therefore,

$$\mathrm{Cov}(z_s^*,\zeta_s|\mathcal{D}) = E\left\{ \frac{1}{N_s} \sum_{k=1}^{N_s} \sum_{i=1}^{n_r} [\lambda_i(S_k) - \lambda_i(\mathcal{D})] z_i \right.$$

$$\left. \left[\frac{1}{s} \int_{\mathbf{x} \in S_{k-\mathbf{d}}} z(\mathbf{x})\, d\mathbf{x} - \frac{1}{D} \int_{\mathbf{x} \in \mathcal{D}_{-\mathbf{d}}} z(\mathbf{x})\, d\mathbf{x} \right] \right\}.$$

This can be developed in terms of the variogram

$$\mathrm{Cov}(z_s^*, \zeta_s|\mathcal{D}) = \frac{1}{N_s} \sum_{k=1}^{N_s} \sum_{i=1}^{n_r} [\lambda_i(S_k) - \lambda_i(\mathcal{D})][\overline{\gamma(i,\mathcal{D}_{-\mathbf{d}})} - \overline{\gamma(i,S_{k-\mathbf{d}})}]$$

$$= \frac{1}{N_s} \sum_{k=1}^{N_s} \sum_{i=1}^{n_r} \lambda_i(S_k)[\overline{\gamma(i,\mathcal{D}_{-\mathbf{d}})} - \overline{\gamma(i,S_{k-\mathbf{d}})}] - \sum_{i=1}^{n_r} \lambda_i(\mathcal{D})\left[\overline{\gamma(i,\mathcal{D}_{-\mathbf{d}})} - \frac{1}{N_s} \sum_{k=1}^{N_s} \overline{\gamma(i,S_{k-\mathbf{d}})} \right],$$

where the second term is zero.

Equation (B1) in appendix B yields, using the matrix notation,

$$\text{Cov}(z_s^*, \zeta_s | \mathcal{D}) = \frac{1}{N_s} \sum_{k=1}^{N_s} \mathcal{L}^{\mathrm{T}}(S_k)[\Gamma(\mathcal{D}_{-\mathbf{d}}) - \Gamma(S_{k-\mathbf{d}})].$$

Finally, Eq. (A1) in appendix A yields

$$\text{Cov}(z_s^*, \zeta_s | \mathcal{D}) = \frac{1}{N_s} \sum_{k=1}^{N_s} \Gamma^T(S_k) \mathcal{K}^{-1}[\Gamma(\mathcal{D}_{-\mathbf{d}}) - \Gamma(S_{k-\mathbf{d}})].$$

$$\text{(D1)}$$

APPENDIX E

Index for a Kriged Reference and a Shifted Simulation

As shown in section 3a, $\sigma^2(\zeta_s | \mathcal{D})$ can be written following Eq. (3). As shown in appendix C, $\sigma^2(z_s^* | \mathcal{D})$ can be written following Eq. (C2). As shown in appendix D, $\text{Cov}(z_s^*, \zeta_s | \mathcal{D})$ can be written following Eq. (D1). The insertion of Eqs. (3), (C2), and (D1) in Eq. (6) yields

$$R_{z^*, \zeta}^2(s) = \frac{\left\{ \sum_{k=1}^{N_s} \Gamma^{\mathrm{T}}(S_k) \mathcal{K}^{-1}[\Gamma(\mathcal{D}_{-\mathbf{d}}) - \Gamma(S_{k-\mathbf{d}})] \right\}^2}{N_s[\overline{\gamma_z(\mathcal{D}, \mathcal{D})} - \overline{\gamma_z(S, S)}] \sum_{k=1}^{N_s} \Gamma^{\mathrm{T}}(S_k) \mathcal{K}^{-1}[\Gamma(\mathcal{D}) - \Gamma(S_k)]}. \qquad \text{(E1)}$$

REFERENCES

Barancourt, C., J.-D. Creutin, and J. Rivoirard, 1992: A method for delineating and estimating rainfall fields. *Water Resour. Res.,* **28,** 1133–1143.

Chiles, J.-P., and P. Delfiner, 1999: *Geostatistics: Modeling Spatial Uncertainty.* Wiley and Sons, 720 pp.

Ducrocq, V., D. Ricard, J.-P. Lafore, and F. Orain, 2002: Storm-scale numerical rainfall prediction for five precipitating events over France: On the importance of the initial humidity field. *Wea. Forecasting,* **17,** 1236–1256.

Huttenlocher, D. P., R. H. Lilien, and C. F. Olson, 1999: View-based recognition using an eigenspace approximation to the Hausdorff measure. *IEEE Trans. Pattern Anal. Mach. Intell.,* **21,** 951–955.

Mason, I., 1989: Dependence of the critical success index on sample climate and threshold probability. *Aust. Meteor. Mag.,* **37,** 75–81.

Matheron, G., 1965: *Les Variables Régionalisées et Leur Estima-tion* (*Regionalized Variables and Their Estimation*). Masson, 305 pp.

Tustison, B., D. Harris, and E. Foufoula-Georgiou, 2001: Scale issues in verification of precipitation forecasts. *J. Geophys. Res.,* **106,** 11 775–11 784.

Venugopal, V. B. S., and E. Foufoula-Georgiou, 2005: A new metric for comparing precipitation patterns with an application to ensemble forecasts. *J. Geophys. Res.,* **110,** D08111, doi:10.1029/2004JD005395.

Wang, Z., and A. C. Bovik, 2002: A universal image quality index. *IEEE Signal Process. Lett.,* **9,** 81–84.

Yates, E., S. Anquetin, V. Ducrocq, J.-D. Creutin, D. Ricard, and K. Chancibault, 2006: Point and areal validation of forecast precipitation fields. *Meteor. Appl.,* **13,** 1–20.

Zepeda-Arce, J., E. Foufoula-Georgiou, and K. Droegemeier, 2000: Space-time rainfall organization and its role in validat-ing quantitative precipitation forecasts. *J. Geophys. Res.,* **105,** 10 129–10 146.